Available online at www.sciencedirect.com
ScienceDirect
Acta Materialia 55 (2007) 3073–3080
Acta MATERIALIA
www.elsevier.com/locate/actamat

Molecular dynamics study on the formation of stacking fault tetrahedra and unfaulting of Frank loops in fcc metals

Tomoko Kadoyoshi [a], Hideo Kaburaki [a,*], Futoshi Shimizu [a], Hajime Kimizuka [b,c], Shiro Jitsukawa [d], Ju Li [e]

[a] Center for Computational Science and e-Systems, Japan Atomic Energy Agency, Tokyo and Tokai, Japan
[b] Engineering Technology Division, The Japan Research Institute, Ltd., Tokyo, Japan
[c] Department of Mechanical Engineering, Osaka University, Osaka, Japan
[d] Nuclear Science and Engineering Directorate, Japan Atomic Energy Agency, Tokai, Japan
[e] Department of Materials Science and Engineering, The Ohio State University, Columbus, OH, USA

Available online 7 March 2007

Abstract

Critical conditions have been determined for intrinsic transformation of a vacancy Frank loop into a stacking fault tetrahedron in a face centered cubic metal by the molecular dynamics method. We found that a stacking fault tetrahedron can be formed from the scalene hexagonal vacancy Frank loops of wide range of sizes due to the dissociation of dislocations. We have also found atomistically the dynamical process in which vacancy and interstitial faulted Frank loops transform into perfect loops by the application of the external shear stress or by raising the temperature. We have determined numerically the critical shear stress and temperature for the initiation of unfaulting. The simulation results clearly unveiled the important role of temperature in the unfaulting mechanism of an interstitial Frank loop.

Keywords: Molecular dynamics; Irradiation; Frank loops; Stacking fault tetrahedron; Unfaulting

1. Introduction

Irradiation of face centered cubic (fcc) metals by charged or neutron particles induces atomic collision cascades, where varieties of defect clusters nucleate from the migration and coalescence of self-interstitial atoms and vacancies. Typical clusters that form from this displacement cascade process are hexagonal dislocation loops called Frank loops containing the stacking fault with the Burgers vector $\frac{1}{3}\langle 1\,1\,1\rangle$. These defects are well observed by transmission electron microscopy [1] and are considered to cause significant effects on irradiation hardening and fracture due to dislocation channeling [2]. It is predicted that unfaulting of Frank loops may lead to the formation of dislocation channeling through the absorption of these unfaulted loops by gliding dislocations [3]. However, detailed mechanistic behavior of these Frank loops is not well known due to the resolution limit of electron microscopy and the applicability of the elasticity theory down to the range of 1–5 nm. We study these processes by the molecular dynamics method. We singled out two elementary processes for interstitial and vacancy Frank loops in fcc metals of Cu and Al. One is the dissociation process of interstitial and vacancy Frank loops, in particular, the formation of a stacking fault tetrahedron (SFT) from a vacancy Frank loop. The other is the unfaulting process of Frank loops, where mechanistic cause of this phenomenon is still unknown. We study this unfaulting process by applying a shear strain to determine a critical shear stress for a vacancy and an interstitial Frank loop. We also raise the temperature and study its effects on the complex unfaulting process.

In fcc metals with low stacking fault energy, a perfect dislocation dissociates into two partial dislocations. In the case of interstitial or vacancy Frank loops produced

* Corresponding author.
E-mail address: kaburaki.hideo@jaea.go.jp (H. Kaburaki).

1359-6454/$30.00
doi:10.1016/j.actamat.2007.01.010

by irradiation, they tend to transform into an energetically favorable state by dissociation. The Frank loop with the Burgers vector $\frac{1}{3}\langle 1\,1\,1\rangle$ extends into other equivalent $\{1\,1\,1\}$ planes by creating energetically favorable stair-rod and Shockley partial dislocations. In particular, SFT's, consisting of stair-rod dislocations and the stacking faults, are the typical irradiation induced defects in fcc metals. There are some mechanisms proposed for the creation of SFT's, but we have not obtained a definite answer for this process. One possible scenario is the Silcox–Hirsch mechanism [4,5] where an SFT is formed from an equilateral triangular vacancy Frank loop by dissociation. The former numerical simulations confirm this mechanism by forming an SFT starting from an equilateral triangular plate [6,7]. In this paper, we also confirm the formation of a perfect SFT from an equilateral triangular vacancy loop and, depending on the stacking fault energy, we show firstly that the incomplete SFT is obtained by the molecular dynamics method. However, in the real irradiation cascade process, it is improbable that SFT's are created from equilateral triangular vacancy Frank loops. On the other hand, there are many hexagonal Frank loops developed under the irradiation conditions, and in the process of formation of vacancy Frank loops we try to find a critical condition whether it develops into a dissociated loop or an SFT. We determine the critical condition for the formation of an SFT from an scalene hexagonal Frank loop.

On the other hand, with increasing the size of the faulted loop, there is some point that the elastic energy of the faulted dislocation loop becomes larger compared with the unfaulted perfect dislocation loop. This means that the unfaulted dislocation loop is energetically favorable with increasing size. However, many large-sized faulted Frank loops, observed by the transmission electron microscopy, remain faulted and unfaulting condition is not clearly known. There seems to be some energy barrier for this transformation. In this paper, we determine this energy barrier by applying the external shear stress and raising the temperature of the system. In particular, we focus on the important role of temperature for the unfaulting process of an extrinsic Frank loop, which is found to be hard to unfault by the application of the shear stress.

2. Computational methods

We have employed the recently developed parallel molecular dynamics program, called Parallel Molecular Dynamics Stencil (PMDS) [8], combined with the visualization program of atomistic particles, called AtomEye [9,10,8], to be able to delve into complex defect structures. Our computational region is a rectangular cell consisting of 3.84×10^5 or 1.7×10^6 particles where a defect cluster is placed in the center. The size of the region for the x, y, and z directions ($[1\,1\,0]$, $[\bar{1}\,1\,2]$, $[1\,\bar{1}\,1]$, respectively) is $200\ \text{Å}\times170\ \text{Å}\times120\ \text{Å}$ or $340\ \text{Å}\times300\ \text{Å}\times280\ \text{Å}$.

We have employed two types of methods to apply a shear stress to the system. The first method (shear mode I) is that the upper wall is displaced in the positive x-direction while the lower wall is displaced in the opposite direction at a constant rate. The boundary conditions for the shear mode I case are periodic in the x and y-directions, while the upper and lower sheet in the z-direction are fixed. In the second case (shear mode II), both the right and left side walls along the z-axis are inclined in the x-direction, thus generating the same shear strain as that of shear mode I. The boundary conditions for the shear mode II case are periodic in the y-direction and free in the z-direction on the upper and lower walls. In both cases, it takes time for the linear shear strain to establish throughout the crystal.

Standard molecular-dynamics techniques in the parallel computing environment using the PMDS are applied to integrate the Newton's equation of motion. The time step is basically 2 fs. We have employed the embedded-atom method (EAM) potential [11,12] for interatomic interactions of copper and aluminum. Also, by employing the coordination number and central symmetry parameter representations using the AtomEye, we have successfully visualized clear and detailed dislocation core structures that have not been explored before [10,8]. In the coordination number representations, the atoms are colored according to the coordination number of neighbor atoms, for example, red for 11, blue for 13, and green for 10. The atoms with the coordination number of 12, which corresponds to the perfect fcc crystal, are omitted or transparent in the visualization. The central symmetry parameter is the absolute value of the added displacement vectors for neighbor atoms. This method, which can distinguish between the fcc and hcp structure, is suited to represent a stacking fault in fcc crystals.

3. Simulation results

3.1. Dissociated structures of Frank loops

We study first the intrinsic morphological transformation of a vacancy and an interstitial hexagonal Frank loop of copper due to dissociation. The observations of the irradiated and quenched fcc metals show that interstitials and vacancies aggregate to form hexagonal planar Frank loops on the $\{1\,1\,1\}$ planes with their sides along the $\langle 1\,1\,0\rangle$ directions. Therefore, we start our molecular dynamics simulations with hexagonal loops containing 37–1801 vacancies and 7–10,981 interstitials at 0 K. Fig. 1 shows the relaxed state of dissociation for the copper hexagonal Frank loops consisting of 1801 vacancies and 10,981 interstitials at approximately 7 ps.

It is found that vacancy hexagonal loops tend to be easily dissociated acutely onto the other slip planes equivalent to the $(1\,\bar{1}\,1)$ plane up to the size as shown in the figure. Considering the equivalent $\{1\,1\,1\}$ slip planes, a Shockley partial dislocation is alternately emitted acutely from the sides of the hexagonal loop forming a stacking fault behind, and the dislocation of $\frac{1}{3}\langle 1\,1\,1\rangle$ along the sides of the loop becomes a stair-rod dislocation. On the other

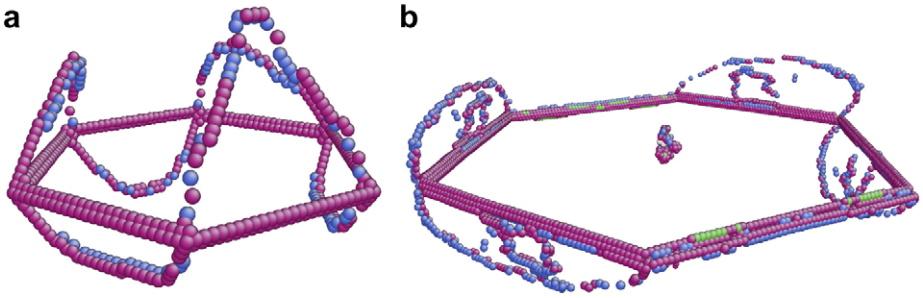

Fig. 1. Dissociation of vacancy and interstitial Frank loops of copper.

hand, we have observed that an interstitial loop is hardly dissociated for smaller sizes. It is firstly visibly dissociated by increasing the size up to 10981 interstitials. In this particular case of the maximum interstitial loop, the computational region is enlarged to the system of 3.46×10^6 particles. It is noteworthy in Fig. 1b that dissociation occurs twice on the $(1\,\bar{1}\,1)$ equivalent planes. It is seen that the first Shockley partial creates an intrinsic stacking fault and the following second partial removes it. Since an interstitial dislocation loop on the $(1\,\bar{1}\,1)$ plane is extrinsic, a dislocation at the junction between the intrinsic and extrinsic stacking fault becomes of the type $\frac{1}{6}\langle 1\,1\,4\rangle$. After the second partial sweeps the stacking fault and leaves a perfect crystal behind, a dislocation of the side of the hexagon becomes a stair-rod of the type $\frac{1}{6}\langle 1\,1\,0\rangle$.

3.2. Formation of stacking fault tetrahedron

Next we study the formation of a stacking fault tetrahedron from an equilateral triangular vacancy plate on the $(1\,\bar{1}\,1)$ plane to confirm the Silcox and Hirsch mechanism [5]. Fig. 2 shows a stacking fault tetrahedron formed from the equilateral triangular plate containing 253 vacancies of copper and aluminum. We found that a perfect tetrahedron is formed for copper, where the sides of which consisting of stair-rod dislocations are represented well by the coordination number representations. On the other hand, in the case of high stacking fault energy of aluminum, a tetrahedron is found to be incomplete for this size, and the top Shockley partial dislocations of the truncated tetrahedron become concave and end upward at the junctions with the stair-rod dislocations [13] due to the high surface tension of the stacking fault. The minimum critical size for the formation of an incomplete tetrahedron of aluminum is found to be an equilateral triangular vacancy plate with 153 sites. All the triangular vacancy plates under this size lead to the formation of a complete stacking-fault tetrahedron. We found that the temperature affects significantly the formation process of a tetrahedron. We observed that a complete tetrahedron is formed even starting with an equilateral triangular vacancy plate with 153 sites by raising the temperature to 100 K.

Formation process of a stacking fault tetrahedron still remains a problem whether it is created directly from precipitation of vacancies or from an equilateral triangular plate of vacancies. Here, we present one possible numerical scenario for the creation of a tetrahedron from a scalene hexagonal vacancy dislocation loop with two different sides. This condition of a hexagonal loop can be realized by the inhomogeneous absorption of glissile interstitials or vacancies. As we have seen in the results of Fig. 1a, a stacking fault tetrahedron cannot be formed from an equilateral hexagonal vacancy loop by dissociation. However, we have found that an incomplete stacking fault tetrahedron is formed as shown in Fig. 3, if we start from the scalene hexagonal vacancy loop of copper whose sides consisting of two different lengths of d_s and d_l. It is predicted in some textbooks on dislocation that a complete tetrahedron can be formed even starting from a scalene hexagonal vacancy loop. It is noted from our numerical

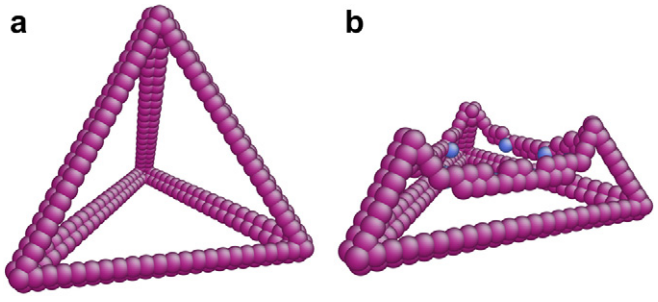

Fig. 2. Formation of tetrahedron for (a) Cu and (b) Al starting from an equilateral triangular plate containing 253 vacancies.

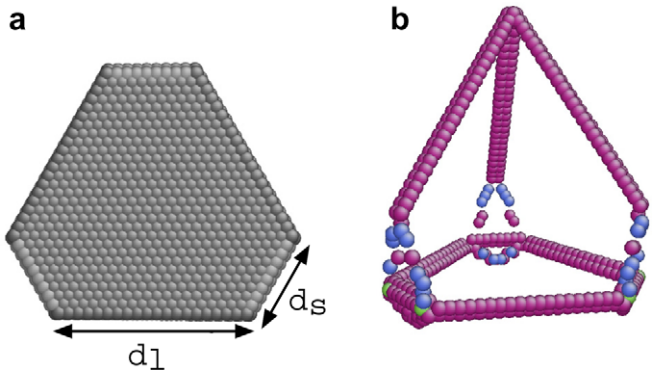

Fig. 3. Formation of an incomplete stacking fault tetrahedron from the scalene hexagonal vacancy loop with two different sides.

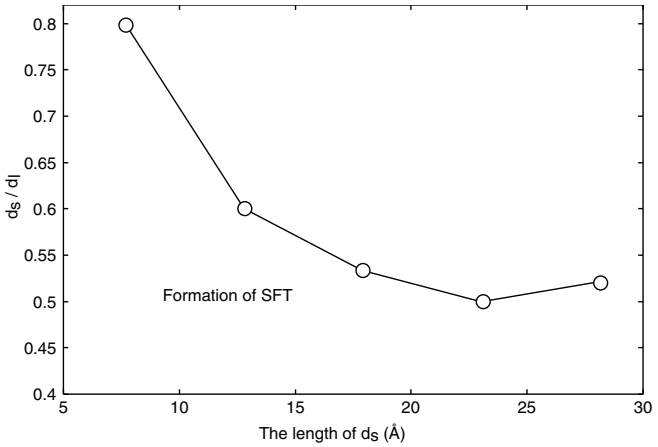

Fig. 4. The condition for the formation of a stacking fault tetrahedron from the scalene hexagonal loop in Cu. The effect of the ratio of the short (d_s) to the long (d_l) side of the hexagonal loop.

results in Fig. 3 that the Shockley partial dislocations generated from the long sides of a loop combine to form stair-rod dislocations, however, they cannot be completely fastened to form an apex at the foot of a tetrahedron. A critical condition for a formation of a tetrahedron from a scalene hexagonal vacancy loop is summarized in Fig. 4. The condition depends on the ratio of the short side to the long side of a loop and the absolute length of the short side of a loop. Formation of a tetrahedron is always observed under the condition which corresponds to the parameter region below the curve in Fig. 4. Generally, a stacking fault tetrahedron always forms if the ratio d_s/d_l is under 0.5. As the size of a loop decreases, a tetrahedron can be formed from nearly a perfect hexagonal loop. The ratio reaches to the value of 0.8 for the minimum size considered here.

3.3. Unfaulting of Frank loops

Observations of interstitial and vacancy Frank loops by the electron microscopy show that some of them are unfaulted, that is, a stacking fault inside a loop is removed and a sessile Frank loop of the Burgers vector $\frac{1}{3}\langle 1\,1\,1\rangle$ transforms into a glissile perfect dislocation loop of $\frac{1}{2}\langle 1\,1\,0\rangle$. On the basis of the elasticity theory, the energy of the perfect loop becomes smaller than that of the Frank loop if the loop size exceeds some critical limit. In particular, in the case of aluminum of high stacking fault energy, the perfect loop is favorable energetically for any size of a dislocation loop [14]. Our molecular dynamics results using the aluminum EAM potential indicate that only increasing the size does not make a loop unfault at 0 K. Also, in experiments by electron microscopy, we observe frequently large-sized faulted Frank loops. It is predicted that there exists some energy barrier for the transformation of a Frank loop. The mechanism for the transformation into a perfect dislocation loop is predicted theoretically that a Shockley partial is created and sweeps across the loop to remove the stacking fault. In a case of a vacancy Frank loop, only one partial is needed to eliminate the fault, while two partials are required for an interstitial Frank loop. However, we have not yet obtained any numerical evidence on how the unfaulting occurs using atomistic methods. The process of unfaulting still remains unexplained. There are two mechanisms, mechanical stress and thermal activation, to be considered for the unfaulting of Frank loops. Here, we study these two effects on the unfaulting of Frank loops and determine their critical shear stress and temperature. Firstly, we study the mechanical stress by applying the external shear strain at 0 K and determine the critical shear stress for unfaulting using the molecular dynamics method with the aluminum EAM potential [12]. The shear stress is measured by using the atomic-level stress tensor derived from the virial formula for the instantaneous pressure function [15]. The atomic-level stress tensor $\sigma_{\alpha\beta}$ for one atom is described by

$$\sigma_{\alpha\beta} = \frac{1}{V}\sum_{i=1}^{N}(mv_\alpha v_\beta + r_\alpha f_\beta), \tag{1}$$

where $\sigma_{\alpha\beta}$ is the stress component α and β ($\alpha,\beta = x,y,z$), V the volume of the target region, N the number of atoms, m the mass of the atom, v_α an α component of a velocity of the atom, r_α an α component of a coordinate of the atom, and f_β a β component of a force on the atom due to the other atom.

We have observed the unfaulting process for both vacancy and interstitial Frank loops under different shear strain rate conditions, and successfully detected the critical initiation of unfaulting using the visualization method.

We have employed two types of methods, shear mode I and II, to apply the shear strain to the system. The real strain rate employed in experiment is too slow to be realized in the molecular dynamics simulations. For both of these modes, we have adopted three shear strain rates of 6.0×10^9/s, 6.0×10^8/s and 6.0×10^6/s. These values are too fast compared to the experimental conditions. We measure global and local shear stresses to validate these values of shear strain rates. As shown in Fig. 5, the global and

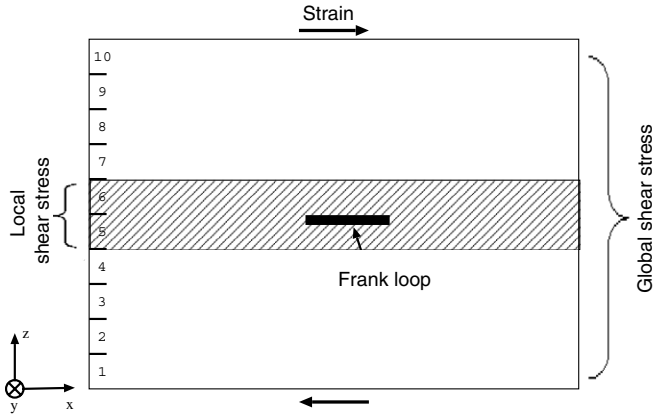

Fig. 5. The global shear stress and local shear stress.

local shear stresses are defined in such a way as to average the atomic-level stress tensor over the whole computational region and the thin region, respectively. Regardless of the shear modes and the shear strain rates, all the measured global shear stresses show a linear relationship in the stress–strain curve corresponding to the slowest shear strain rate of 6.0×10^6/s as shown in Fig. 6. The local shear stress shows a variation depending on the shear strain rates. In the case of fast shear strain value of 6.0×10^9/s, the local shear stress varies stepwise, which indicates that the disturbance from the upper wall propagates like a pulse and the abrupt shear stress incurs on the defect. This condition may lead to a different phenomenon concerning the unfaulting process of a dislocation loop, comparing with the slow strain rate condition. The shear strain rate of 6.0×10^6/s is found to be appropriate for the simulation condition because the measured local and global shear stress almost coincide. However, in the present computing environment, the shear strain rate of 6.0×10^6/s is too demanding for a parametric study of many simulation cases. Therefore, we basically employ the shear strain rate of 6.0×10^8/s and confirm partially with the shear strain rate of 6.0×10^6/s that the both cases give almost the same result. Critical unfaulting shear stresses for a vacancy and an interstitial Frank loop have been measured at 0 K under two shear modes I and II with three, fast, medium, and slow shear strain rates. The unfaulting shear stress is determined by visualizing the Frank loop and confirming the disappearance of the inner stacking fault. The Frank loops under study are hexagonal-shaped vacancy and interstitial faulted loops, whose diagonal length ranges from 40 Å to 137 Å. All the conditions of numerical simulations and the measured results for the final state of the Frank loop are summarized in Table 1. As indicated in Table 1, we found that vacancy loops of any size transform into unfaulted perfect dislocation loops under any conditions of shear strain modes and rates. Under the shear mode I, the interstitial loops become unfaulted with the fast shear strain rate, however, remain faulted with the medium shear strain rate. Under the shear mode II, unfaulting of the interstitial loops is observed for several cases with the slow shear strain rate. In the case of shear mode I, the length of the region in the z-direction is fixed and then the interstitial loop is inserted, which induces a compressive stress on both sides of the loop and inhibits the generation of dislocations to sweep out the stacking fault. On the other hand, the compressive stress is relaxed due to the free surface condition of the upper and lower walls for the shear mode II, which makes it easier to generate dislocations in some cases. However, although the inside stacking fault of the interstitial loop is swept out by partial dislocations, the final unfaulted state is found to be not the glissile $\frac{1}{2}\langle1\,1\,0\rangle$ dislocation. It is concluded that the interstitial loops do not transform into perfect glissile dislocation loops under the application of the uniform external shear stress.

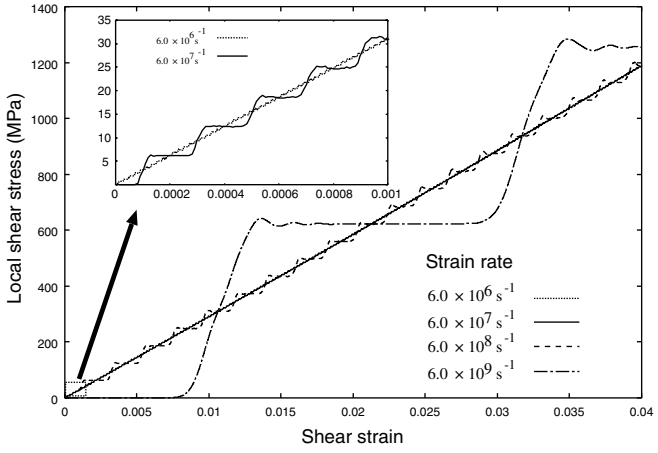

Fig. 6. The local stress–strain relation for the fast (6.0×10^9/s), medium (6.0×10^8/s), and slow (6.0×10^6/s) shear strain rate conditions.

Fig. 7a and c shows respectively the unfaulting process for a vacancy and interstitial Frank loop using the coordination number representation under the shear stress conditions. For a vacancy Frank loop containing 721 lattice sites, two circular partials are created across the diagonal line of the hexagon, and these partials are enlarged to eliminate the stacking fault. For vacancy Frank loops with smaller size, we found that only one circular partial is created in the center of the hexagon and unfaulting results. Since the coordination number representation cannot

Table 1
The unfaulting status of vacancy and interstitial Frank loops under the shear strain condition studied by the molecular dynamics simulation

	Number of lattice sites	169	217	331	397	469	547	721	1141	1801
	Diagonal length (Å)	40	45	57	62	68	74	85	108	137
V-loop	I (F,M)	○	○	○	○	○	○	○	○	○
	II (M,S)	○	○	○	○	○	○	○	○	○
I - loop	I (F)	△	△	△	△	△	△	△	△	△
	I (M)	×	×	×	×	×	×	×	×	×
	II (M)	×	×	△	×	×	×	△	△	×
	II (S)	–	–	×	–	–	–	×	×	–

The diagonal length means the length between distant vertices in the hexagon. Numbers I and II indicate the shear mode I and II, and symbols F, M and S represent the fast, medium, and slow shear strain rates of 6.0×10^9/s, 6.0×10^8/s, sand 6.0×10^6/s. The symbol ○ indicates that the unfaulting state is obtained leading to a perfect glissile dislocation loop. The symbol △ means that the stacking fault is unfaulted while a dislocation loop remains to be sessile. A dislocation loop remains faulted for the symbol ×.

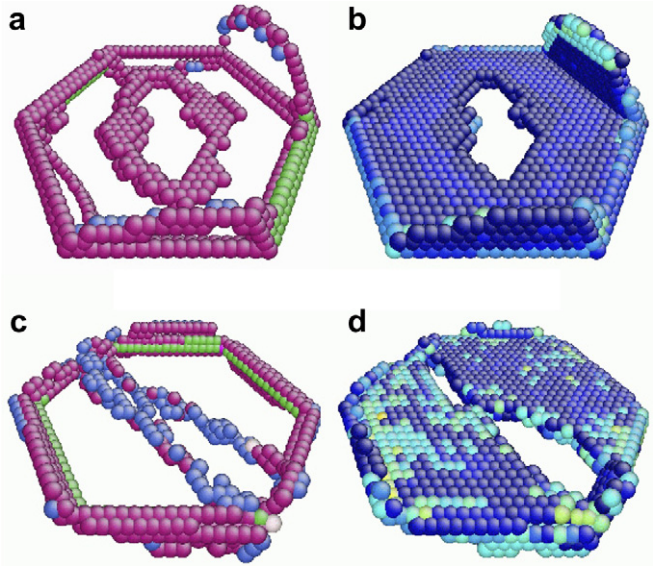

Fig. 7. Unfaulting process of a vacancy and an interstitial Frank loop of aluminum containing 721 lattice sites under the shear strain condition. A vacancy and an interstitial loop are visualized in coordination number representation in figures (a) and (c), and in a central symmetry parameter representation in figures (b) and (d).

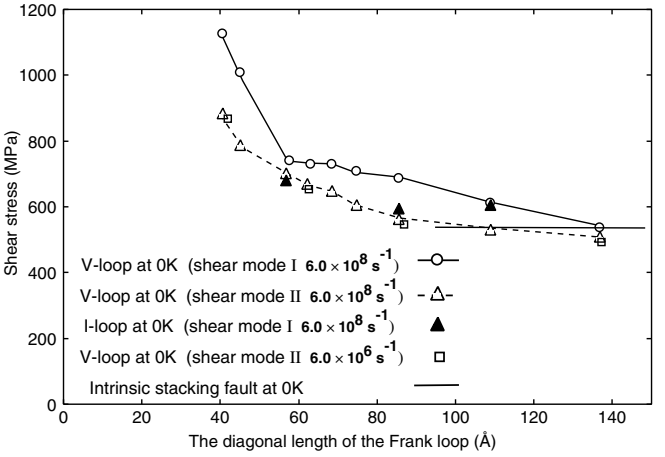

Fig. 8. Critical shear stress for the initiation of unfaulting of a vacancy Frank loop (V-loop), an interstitial Frank loop (I-loop), and an intrinsic stacking fault for aluminum.

distinguish between an fcc and hcp structure, a central symmetry parameter representation is used to confirm the unfaulting state as shown in Fig. 7b and d. They clearly indicate that unfaulting occurs. For an interstitial Frank loop containing 721 lattice sites as shown in Fig. 7c and d, we observe that two partials are emitted from the opposite corners of the hexagon respectively, and unfaulting occurs when they meet and cross each other, that is, the stacking fault is doubly swept by partials. As indicated in the last paragraph, the final state of the interstitial loop is not the glissile $\frac{1}{2}\langle 1\,1\,0\rangle$ dislocation. In this process of unfaulting, we observe a small total temperature rise of approximately 0.1 K in this system due to the movement of a Shockley partial dislocation. This temperature rise depends on the length of a dislocation and the size of the total system. Moreover, it takes approximately 0.8 ps from the initiation of unfaulting to the final perfect loop state. The time also depends on the size of the loop.

The critical shear stress for the onset of unfaulting, measured using the middle and slow shear strain rate of 6.0×10^8/s and 6.0×10^6/s for vacancy Frank loops under the shear mode I and II conditions and interstitial Frank loops under the shear mode II, is summarized in Fig. 8. We found that the values of critical shear stress of unfaulting for vacancy and interstitial Frank loops are almost the same. And in the case of vacancy Frank loops, it is noted that the medium and slow shear strain rates give mostly the same unfaulting properties. We observe generally that the critical shear stress decreases as the size increases, and the curves converge to the observed value of unfaulting for the entire intrinsic stacking fault where the whole $(1\bar{1}1)$ plane is set faulted with no dislocation boundaries. This numerical value of 550 MPa comes very close to the value estimated from the reported values of the EAM potential [12] where the intrinsic stacking fault energy is 146 [mJ/m^2] and the unstable stacking energy is 168 [mJ/m^2].

There are many observations of unfaulting using the electron microscopy, for example, the faulted Frank loops in quenched aluminum [16]. It is estimated in these papers that a shear stress necessary for unfaulting is approximately several to ten percent of the shear modulus, which agree roughly with the present results. Quantitative measurements of the unfaulting shear stress are meager except for the case of the interstitial Frank loop in nickel [17]. The reported value of the critical shear stress for unfaulting is predicted to be approximately 3.7 MPa for nickel at 723 K, which is very low. Considering the results of Fig. 8, that an interstitial Frank loop is hard to unfault by a shear strain, a very small shear stress obtained here may be due to the temperature effect described below.

The effect of temperature on the unfaulting of an interstitial Frank loop containing 1801 lattice sites has been studied using a system consisting of approximately 1.7×10^6 particles. All the boundaries of the simulation region are set as a free condition to accommodate the thermal expansion due to the temperature increase. The target temperature of the region is achieved by the velocity scaling method with the temperature increase rate of 0.5 K/ps. The whole system is controlled at the constant temperature to study the unfaulting process of the interstitial loop. The period of observation at the constant temperature is at the most 80 ps. The unfaulting of the interstitial loop is not observed until the temperature up to 90 K. As shown in Fig. 9, at 100 K, an emission of a first partial dislocation is observed in the center of the interstitial loop at 32 ps after the observation starts, and the unfaulting is completed during nearly 14 ps through a very complex process.

We found that the transformation of an interstitial faulted loop into a perfect glissile loop is realized only by the effect of temperature and without the applied shear

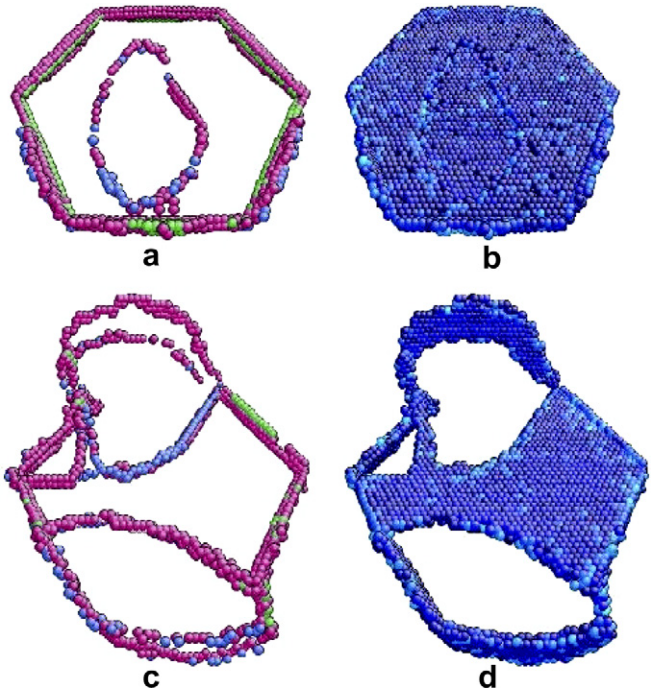

Fig. 9. Molecular dynamics results for the unfaulting process of the interstitial Frank loop with 1801 lattice sites at 100 K. A first partial dislocation is created at 1 ps for (a) and (b), and unfaulting begins around 8 ps for (c) and (d). The figures (a) and (c) are represented by a coordination number, and (b) and (d) by a central symmetry parameter.

stress. The critical temperature of unfaulting for the interstitial loop with 1801 lattice sites is found to be approximately 100 K. In the case of the vacancy Frank loop consisting of 1801 lattice sites, we found the unfaulting is observed at the lower temperature of approximately 30 K. In this case, the unfaulting process is the same as that by the applied shear stress.

The detailed processes of unfaulting for a vacancy and an interstitial Frank loop are described in the following way. In the case of an fcc crystal, there are two types of stacking faults, intrinsic and extrinsic, corresponding to a vacancy and an interstitial Frank loop, respectively. There is one break in the stacking sequence of an intrinsic loop, while there are two breaks in an extrinsic loop. Therefore, one partial dislocation is required to transform an intrinsic loop into a perfect loop by sweeping across the stacking fault, while two partial dislocations are required for an extrinsic loop.

In the case of a vacancy Frank loop, one partial dislocation is generated and sweeps up the stacking fault, and finally a glissile dislocation loop of $\frac{1}{2}\langle 1\,1\,0\rangle$ is obtained by combining a partial dislocation and a vacancy Frank loop. In this process, any one partial dislocation of the type $\frac{1}{6}\langle 1\,1\,2\rangle$ among the three different partials a, b, c on the $\{1\,1\,1\}$ plane, as shown in Fig. 10, can combine with a Frank partial to generate a perfect dislocation loop. On the other hand, in the case of an interstitial Frank loop, two partials combine with a Frank partial to generate a glissile perfect loop. In this process, two different partial

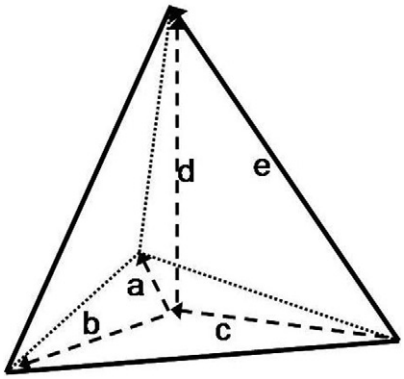

Fig. 10. The Thompson tetrahedron and three different $\frac{1}{6}\langle 1\,1\,2\rangle$ partials a, b, c on the $\{1\,1\,1\}$ plane.

dislocations of the type $\frac{1}{6}\langle 1\,1\,2\rangle$ are required. As shown in Fig. 10, for example, partial dislocations a and b are added to generate a partial dislocation c of $\frac{1}{6}\langle 1\,1\,2\rangle$, which combines with a Frank partial d of $\frac{1}{3}\langle 1\,1\,1\rangle$, leading finally to the formation of a perfect dislocation e of $\frac{1}{2}\langle 1\,1\,0\rangle$. This explains why unfaulting for an interstitial loop is not realized under the external uniform shear stress. In the case of uniform fast shear strain rate, it appears that unfaulting occurs by the emission of two partials due to the pulse-like local shear stress. However, a final perfect dislocation is not obtained since two different types of partials cannot be produced under this uniform shear stress condition.

Complex unfaulting processes, corresponding to the molecular dynamics results of Fig. 9, are schematically

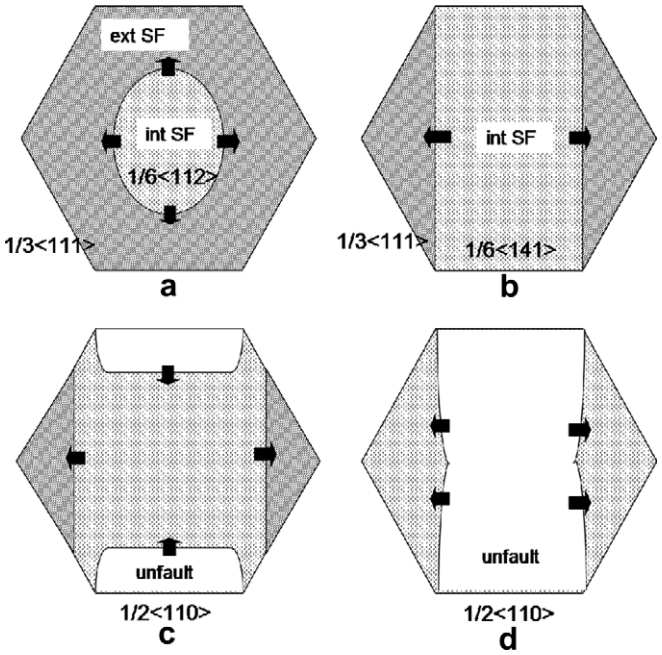

Fig. 11. Schematic diagrams of an unfaulting process of an interstitial Frank loop. The symbols int and ext in the figure represent intrinsic and extrinsic, respectively.

shown in Fig. 11. Since an energy of an extrinsic stacking fault is high, a small partial dislocation is created due to the fluctuations of temperature to produce an intrinsic stacking fault (Fig. 11a). This partial dislocation is enlarged to generate a dislocation of $\frac{1}{6}\langle 1\,4\,1\rangle$ by combining with a Frank loop (Fig. 11b). Since a dislocation of $\frac{1}{6}\langle 1\,4\,1\rangle$ is equivalent energetically to a dislocation of $\frac{1}{2}\langle 1\,1\,0\rangle$, a partial dislocation of $\frac{1}{6}\langle 1\,1\,2\rangle$ is likely to be emitted, and this sweeps up the intrinsic stacking fault (Fig. 11c). Finally, the unfaulting completes by sweeping out the remaining stacking fault (Fig. 11d).

In summary, we have studied dynamical processes of the transformation of the Frank loops, which have not been unexplored by experiments, by the molecular dynamics method combined with the visualization. In particular, we have demonstrated the formation process of a stacking fault tetrahedron from the scalene hexagonal vacancy dislocation loop and the unfaulting process of a vacancy and interstitial Frank loop by the application of the external shear stress. We also unveiled the complex mechanism of unfaulting for an interstitial Frank loop by raising the temperature.

Acknowledgement

H.K. and J.L. express their thanks to Sidney Yip for discussions of the molecular dynamics method.

References

[1] Eyre BL, Loretto MH, Smallman RE. In: Smallman RE, Harris JE, editors. Vacancies '76. London: The Metals Society; 1977. p. 63.
[2] Fish RL, Hunter CW. Irradiation effects on the microstructure and properties of metals. ASTM STP 611. American Society for Testing and Materials; 1976. p.119–38.
[3] Rodney D. Acta Mater 2004;52:607.
[4] Silcox J, Hirsch PB. Philos Mag 1959;4:72.
[5] Amelinckx S. Dislocations in solids 2. Oxford: North-Holland Publ. Co.; 1979.
[6] Osetsky YN, Serra A, Victoria M, Golubov SI, Priego V. Philos Mag A 1999;79(9):2259.
[7] Wirth BD, Bulatov V, Diaz de la Rubia T. J Nucl Mater 2000;283–287:773.
[8] Kimizuka H, Kaburaki H, Shimizu F, Li J. Computer-Aided Mater Des 2003;10:143.
[9] Li J. Model Simul Mater Sci Eng 2003;11:173.
[10] Li J, Krystyn J, Zhu T, Yip S, Suresh S. Nature 2002;418:307.
[11] Mishin Y, Mehl MJ, Papaconstantopoulos DA, Voter AF, Kress JD. Phys Rev B 2001;63:224106.
[12] Mishin Y, Farkas D, Mehl MJ, Papaconstantopoulos DA. Phys Rev B 1999;59:3393.
[13] Humble P, Segall RL, Head AK. Phil Mag 1967;15:281.
[14] Hull D, Bacon DJ. Introduction to dislocations. 4th ed. Oxford: Butterworth-Heinemann; 2001.
[15] Allen MP, Tildesley DJ. Computer simulation of liquids. Oxford University Press; 1987.
[16] Kiritani M, Yoshida S, Shimomura Y. J Phys Soc Jpn 1963; 18(Suppl. III):47;
Edington JW, Smallman RE. Phil Mag 1965;11:1089.
[17] Jitsukawa S, Katano Y, Shiraishi K. J Nucl Sci Tech 1984;21(9):671.